Journal of Scientific & Industrial Research
Vol. 85, June 2026, pp. 491-500
DOI: 10.56042/jsir.v85i6.19444

Enhancing Performance of a PERC Type Solar Cell Utilizing Improved Laser Ablation Techniques

Devdutt Singh[1,2]*, S. R Meka[1], B. K Pant[2] & Himadri Agarwal[2]

[1]Metallurgical & Materials Engineering, Indian Institute of Technology, Roorkee 247 667, India
[2]Bharat Heavy Electricals Limited, New Delhi 110 003, India

Received 06 May 2025; revised 01 January 2026; accepted 04 August 2026

This study has attempted to build understanding of the effect of laser parameters including laser energy, pulse duration, and beam size on dielectric ablation characteristics for Passivated Emitter Rear Cell (PERC) type solar cells. The investigated composite dielectric layer consists of the bottom Al−oxide layer (~20 nm) and the top Si−nitride layer (~70 nm) with an interlayer of Si−oxynitride (~25 nm). Dielectric layers were deposited using PECVD on a monocrystalline (100) Si wafer and contacts were made by screen printing utilizing Ag paste on the front side and Al paste on the rear side. Different contact geometries were created to understand the effect of contact geometry on ablation−induced metallurgical damage and thus on the performance of cells. The study indicated that the usage of Ultraviolet picosecond laser with a dash contact pattern resulted in the highest cell efficiency over 22%. Other laser energies (Infrared, Green) with pulse duration (nanoseconds, picoseconds, and femtoseconds) either led to more damage or incomplete contact opening. The extent and area of ablation−induced damage to the substrate showed dependence on the contact pattern/geometry chosen, the spot−size and spot overlapping criteria followed. This study has presented a detailed discussion for recommending an optimized rear contact pattern geometry and laser ablation parameters considering metallurgical damages, the charge collection area and minority carrier lifetime of the fabricated PERC type solar cell.

Keywords: Dielectric ablation, Kirkindal void, Laser contact opening, Laser fluence, Minority carrier lifetime

Introduction

Laser ablation has been widely used as a surface modification/texturing technique to enhance the performance of solar cells, including Passivated Emitter and Rear Cell (PERC) solar cells.[1,2] By using laser ablation, micro and nanostructures can be generated on the silicon wafer's surface, leading to improved light absorption and reduced reflectivity, resulting in an overall increase in efficiency.[3] Studies have shown that laser ablation can improve the efficiency of PERC solar cells by up to 0.7% compared to laser texturing.[4–5] This improvement is attributed to increased light trapping, enhancing light absorption in the silicon material.[4] Additionally, laser−induced microstructures can reduce the surface reflectance of the silicon wafer by up to 90%, further increasing the solar cell's efficiency.[2–5]

Laser ablation is extensively used to selectively remove the dielectric layer on the back surface of the PERC solar cell, enhancing its efficiency by up to 1.7% compared to conventional Al−BSF solar cells.[6] This technique allows the creation of a Local Back Surface Field (LBSF), which reduces surface recombination velocity and increases the cell's open−circuit voltage. It involves using a laser beam to selectively remove material from a substrate, leaving a patterned surface. In a study by David *et al.*[7] laser ablation was found to significantly improve PERC solar cell's efficiency by removing the passivation layer from the back surface, allowing for better charge carrier collection. Similarly, Sato *et al.*[8] & Wu *et al.*[9] found that laser ablation could improve PERC solar cell's efficiency by up to 0.6% compared to standard BSF cells. Jaeger *et al.*[10] studied the passivation characteristics of AlO_x layer upon laser ablation. However, there are some shortcomings associated with laser ablation in PERC solar cells, such as the cost of the process and potential damage to the cell, reducing its overall efficiency.

In terms of the geometry and area of laser ablation, several studies have shown that the size and shape of the ablated area can significantly affect the solar cell's performance. Suh *et al.*[11] found that an optimized laser ablation pattern could increase a PERC solar cell's efficiency by up to 0.2%. Kim *et al.*[12] found that increasing the width of the laser ablation area could

*Author for Correspondence
E-mail: singh.devdutt@gmail.com

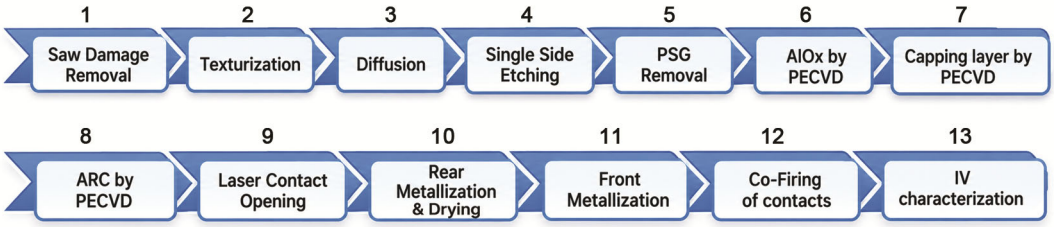


Fig. 1 — Comeplete process flow for manufacturing of PERC solar cells.

decrease the solar cell's short−circuit current. Opening ratio (Laser contact opening) of 5% using dash pattern with dash to gap ratio of 2:1 resulted in efficiency of 20.6% (Mono PERC).[13,14] Dash to gap ratio of 1:1, 2:1, 3:1 have been used with opening ratio in the range of 1.66% to 3.98 % and has achieved max efficiency of 20.63% with opening ratio of 1.99% indicating high opening ratio corresponds to high rear charge recombination.[15]

As a consequence of solubility difference between Si in Al and Al in Si, during firing of the contacts Kirkindal voids develop and the number of these voids increases with increasing contact spacing.[16] It is understood from the literature and series of laser ablation experiments that the laser ablation geometry along with opening ratio & dash to gap ratio have critical impact on the performance of a PERC solar cell viz. Fill factor, Minority Carries Lifetime, VoC, Surface recombination velocity etc. It is imperative to study all of these parameters to draw meaningful conclusions after experimental trials and successive measurement of end properties like Minority Carrier lifetime, VoC, Efficiency and External Quantum efficiency of produced PERC type Solar cells.

Laser ablation alone cannot achieve significant efficiency gains; it must be studied alongside contact metallization. Charge collection depends on Al−Si eutectic formation, influenced by firing temperature, paste composition, and cooling media. Cost reduction requires efficient laser sources for mass production. Optimizing laser parameters such as energy, spot size, and scan speed, minimizes metallurgical damage to Si. This study examines dot and dash patterns with varying spot sizes, energies, and geometries to optimize Laser Contact Opening (LCO). Metallization was then optimized to achieve an improved LBSF, enhancing PERC solar cell efficiency.

Process and Experimentation

Typical process steps followed for developing PERC structure on the rear of the regular industrial solar cell is shown below:

Mono−crystalline PERC silicon solar cells were fabricated following the process in Fig. 1. P−type, 158.75 mm² silicon wafers (100 Crystal orientation) were textured in an alkaline solution at 85°C, established by Singh *et al.*[17] The surface reflectance was measured using a QE setup, yielding a weighted average reflectance of 11−12% (400−1000 nm). SEM confirmed uniform pyramids (2−3 µm height), optimized through solution composition, time, and temperature. Phosphorus diffusion was performed in a $POCl_3$ based diffusion furnace at 780−790°C (deposition) and 810–820°C (drive−in), achieving a sheet resistance of 110−120 Ω/□. Measurements were taken via a 4−point probe and Electrochemical Capacitance−Voltage (ECV). Rear−side chemical polishing was conducted using a single−side etching tool, with a water mist spray protecting the front surface. The phosphosilicate glass (PSG) layer served as an emitter protector, while rear−side polishing was optimized using a controlled laminar flow process.

Anti−Reflection Coating (ARC) of Si_xN_y was deposited on the front, while a rear dielectric stack ($AlO_x/SiON_x/Si_xN_y$) was applied via Plasma Enhanced Chemical Vapor Deposition (PECVD). AlO_x was deposited using TMA and N_2O, followed by capping layers of $SiON_x$ and Si_xN_y using silane, ammonia, and N_2O. Secondary Ion Mass Spectroscopy (SIMS) characterized these layers. Optimized wafers were grouped into batches for rear−side dielectric ablation. Laser ablation of dielectric layer was carried out using UV picosecond pulsed laser which is established as most optimized laser ablation source by Singh *et al.*[13] at different laser parameters (laser power, spot diameter, spot overlapping) along with geometrical parameters (dash length, pitch, distance between two dashes, distance between two dots) to find the optimal ablation and geometric parameters to realize the maximum cell efficiency. After laser ablation, metallization was carried to print the contact of front and rear side using a screen printer. Contacts were co−fired in a belt

furnace. Contact printing parameters were also optimized including screen design (number of fingers, bus bars, their width and height using print on print, dual print methodology), paste composition, drying and firing temperature to obtain an efficient PERC type solar cell.

Mono−crystalline PERC silicon solar cells were fabricated following the process in Fig. 1. P−type, 158.75 mm² silicon wafers (100 orientation) were textured in an alkaline solution at 85°C. The surface reflectance was measured using a QE setup, yielding a weighted average reflectance of 11−12% (400−1000 nm). SEM confirmed uniform pyramids (2−3 µm height), optimized through solution composition, time, and temperature. Phosphorus diffusion was performed in a $POCl_3$ based diffusion furnace at 780−790°C (deposition) and 810–820°C (drive−in), achieving a sheet resistance of 110−120 Ω/□. Measurements were taken via a 4−point probe and ECV. Rear−side chemical polishing was conducted using a single−side etching tool, with a water mist spray protecting the front surface. The phosphosilicate glass (PSG) layer served as an emitter protector, while rear−side polishing was optimized using a controlled laminar flow process.

Anti−Reflection Coating (ARC) of Si_xN_y was deposited on the front, while a rear dielectric stack ($AlO_x/SiON_x/Si_xN_y$) was applied via Plasma Enhanced Chemical Vapor Deposition (PECVD). AlO_x was deposited using TMA and N_2O, followed by $SiON_x$ and Si_xN_y using silane, ammonia, and N_2O. Secondary Ion Mass Spectroscopy (SIMS) characterized these layers. Optimized wafers were grouped into batches for rear−side dielectric ablation. Laser ablation of dielectric layer was carried out using UV picosecond pulsed laser[13] at different laser parameters (laser power, spot diameter, spot overlapping) along with geometrical parameters (dash length, pitch, distance between two dashes, distance between two dots) to find the optimal ablation and geometric parameters to realize the maximum cell efficiency. After laser ablation, metallization was carried to print the contact of front and rear side using a screen printer. Contacts were co−fired in a belt furnace. Contact printing parameters were also optimized for paste composition, drying and firing temperature to obtain an efficient PERC type solar cell.

Results and Discussion

Wafer having ARC deposited and laser dielectric stack deposited, were studied under SIMS to characterize the total stack thickness and composition which is formed with thin layers of oxides, oxynitride and nitrides. Different layers of front and rear side dielectric stack of a PERC solar cell are illustrated in the schematic cross−section of cell presented in Fig. 2.

Individual layers were also assessed using spectrometric ellipsometry to optimize the process of deposition using PECVD. SIMS characterization was used to find the approximate thickness of various layers deposited as a dielectric stack. Elemental composition as a function of depth obtained from SIMS measurements presented in Fig. 3 indicated about 20 nm thickness of Aluminum oxide (AlO_x), 25 nm thickness of Silicon oxi−nitride ($Si_xO_yN_z$) and about 70 nm thickness of Silicon nitride (Si_xN_y) with total dielectric stack thickness of about 120 nm.

The thickness and refractive index of layer deposited using PECVD were characterized using spectrometric ellipsometry as shown in Table 1.

While the earlier studies have significantly contributed for the development of the PERC architecture, the present study introduces distinct advances in terms of process integration, contact engineering, co−optimization the parameters and improvement of the other upon feedback from subsequent process.

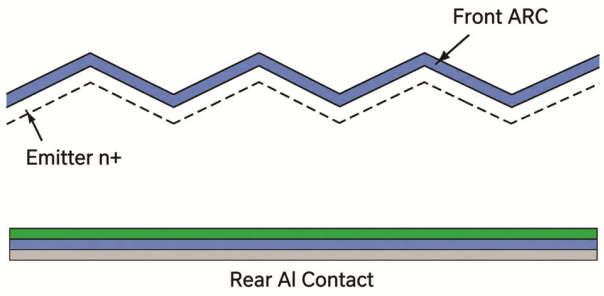


Fig. 2 — Schematic cross−section of PERC type Solar cell: rear surface, Green−AlO_x layer + Blue −Capping layers ($SiON_x$ & SiN_x) + Rear metallization. ARC on textured front side

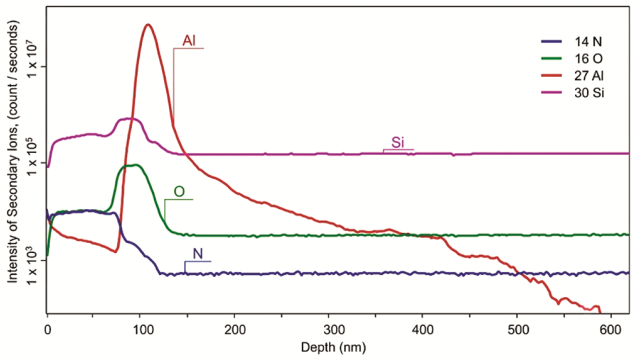


Fig. 3 — SIMS Profile of dielectric layer distinguishing different sub layers

The work by Jaeger & Hezel[10] demonstrate the effect of Al_2O_3, primarily focusing on passivation quality and its impact on MCLT. This study did not address lased contact opening or its interaction with subsequent process of metallization and firing. Kim *et al*.[12] investigated laser ablation of Al_2O_3/SiN_x dielectric stacks in PERC cells, emphasizing on ablation characteristics and process feasibility. While this work provide insights of laser material interaction, but remains focused on ablation quality and did not explore the coupled effect of contact geometry, subsequent metallization and firing optimization. Further, Chiu *et al*.[15] have examined the influence of lased ablated LCO w.r.t. pitch and geometry on cell efficiency. However, it primarily analyses geometrical variation without integrating process dependent parameters such as laser conditions and firing profile.

This study, bridges the gap between isolated laser ablation studies and full cell fabrication establishing a comprehensive, feedback driven optimization of LCO, metallization and firing process, thereby enabling improved contact quality and enhanced cell performance.

Table 1 — Spectrometry Ellipsometry results for RI & layer thickness

Sample No	Process recipe	Ellipsometry Results (Refractive Index)	Ellipsometry Results (Thickness in nm)
1	SiN_x Dual Layer	2.05	56
2	SiN_x single Layer	2.02	76
3	$SiON_x$	2.02	110
4	SiO_x(4 min)	1.44	98
5	SiO_x (6 min)	1.45	106
6	SiO_x (10 min)	1.48	160
7	AlO_x	1.65	106
8	AlO_x + $SiON_x$+ SiN_x	1.65/1.9/2.26	20/25/70
9	SiO_x + SiN_x	1.6/1.92	20/100

In this study, multiple laser processing conditions including IR, Green, UV wavelengths, operated in nanosecond, picosecond, and femtosecond regimes with power levels ranging from 30% to 100%, were performed for Laser contact opening (LCO). A quantitative assessment of LCO was performed to examine the uniformity across the wafer using a combination of microscopy imaging and profilometry measurements at multiple positions (center, middle and edge).

Laser ablation experiments were conducted using various laser regimes and settings. Parameters for line patterns included a line pitch of 0.9 mm, a mark speed of 4 m/s, and a jump speed of 2 m/s. Dash pattern parameters included a pitch of 0.7 mm, a dash length of 0.6 mm, and a dash gap of 0.3 mm. Surface morphologies of ablated regions were studied under SEM to assess laser−induced damage, such as melting, partial melting, recrystallization, or plastic deformation. Trials using 25% laser power with IR (nanoseconds, picoseconds, and femtoseconds) and Green (nanoseconds) lasers revealed melted or partially melted areas with plastically deformed regions. This indicates that IR lasers at 25% power are unsuitable for ablation due to excessive heat generation, though they may be viable for cutting applications with higher power and optimized passes. The observed damage disrupts the monocrystalline structure of the wafer, creating recombination centers that reduce cell efficiency by increasing shunt resistance and lowering series resistance.

Further experiments with higher power levels focused on Green (picosecond and femtosecond) and UV (picosecond and femtosecond) lasers. SEM analysis showed that surfaces ablated with Green and UV femtosecond lasers exhibited minimal damage, confirming their suitability for precise dielectric ablation. Results, documented in Table 2, suggest that

Table 2 — Effect of various laser parameter including laser type on laser contact opening damage

Type of Laser	Laser λ(nm)	Laser pulse	Power (W)	Energy (μ−J)	Power used (%)	Area (mm^2)	Laser Fluence (J/cm^2)	Observation
UV	343	Fs	5.7	57.0	50	0.28	1.01	No melting or Plastic Deformation (Fig. 4a)
	343	Ps	1.18	11.8	100	0.28	0.42	No melting or Plastic Deformation (Fig. 4b)
Green	515	Fs	13.0	130.0	30	0.28	1.38	No melting or Plastic Deformation (Fig. 4c)
	515	Ps	5.9	59.0	40	0.28	0.83	No melting or Plastic Deformation (Fig. 4d)

Green and UV short pulse lasers provide the best outcomes for minimizing substrate damage.

The laser fluence values considered suitable for a good laser surface interaction depend on the type of laser used. For "ns" laser ablation, the ablation process starts when the laser fluence exceeds ~ 5 J/cm^2 whereas for "ps" laser, the laser fluence is ~ 1.2 J/cm^2. For "fs" lasers, it is expected to be < 1 J/cm^2. The different laser fluences have been optimized in this study based on the surface morphology and characteristics corresponding the spotting melting/recrystallization using SEM micrographs (Fig. 4). It is observed that for low damage laser dielectric ablation, surface melting should be avoided, Green & UV−Femtoseconds and picoseconds regimes meets these requirements.

The UV picosecond laser was selected as an optimal trade−off between thermal budget control, ablation precision, and industrial throughput. While femtosecond lasers offers minimal thermal damage its expected higher cost is limiting industrial scalability. Nanosecond lasers, although cost−effective, exhibit larger heat−affected zones. UV picosecond lasers provide sufficient precision with manageable thermal diffusion, making them well suited for high−volume manufacturing.

It is observed that circular contacts of diameters 52 µm and 43 µm were obtained using 40% laser power and 30% laser power, respectively Fig. (5). Laser powers lower than 30% led to improper ablation. Therefore, a spot diameter of 43 µm was chosen to do further experimentations as it will be leading to minimal damaged area while establishing a proper contact with the Si substrate.

A factor that was investigated in this study is the distance between dots which changes the ablation area and thus the cell performance. Distance between dots is varied from 36µm to 76µm (Figs 6a, 6b, 6c) which

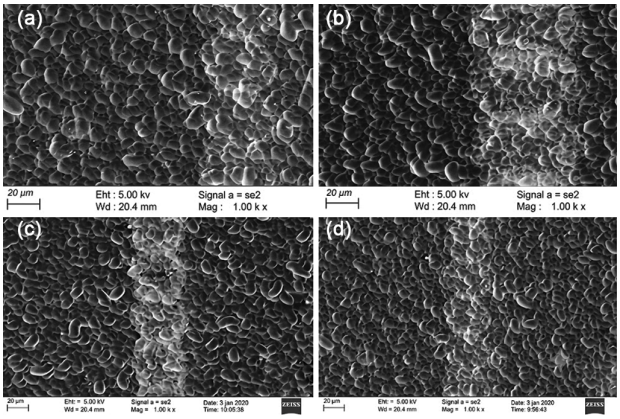


Fig. 4 — Top surface of the LCO with spot size ~ 50 micron with varied power (a) UV "fs" laser with 50% power (b) Green "fs" laser with 40% power (c) Green "fs" laser with 30% power (d) UV "ps" laser with 100% power

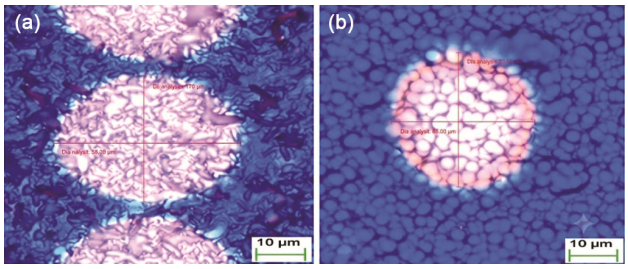


Fig. 5 — Variation of spot diameter with Laser power: (a) 30% Power (Spot diameter− 43 µm), (b) 40% Power (Spot diameter − 52 µm)

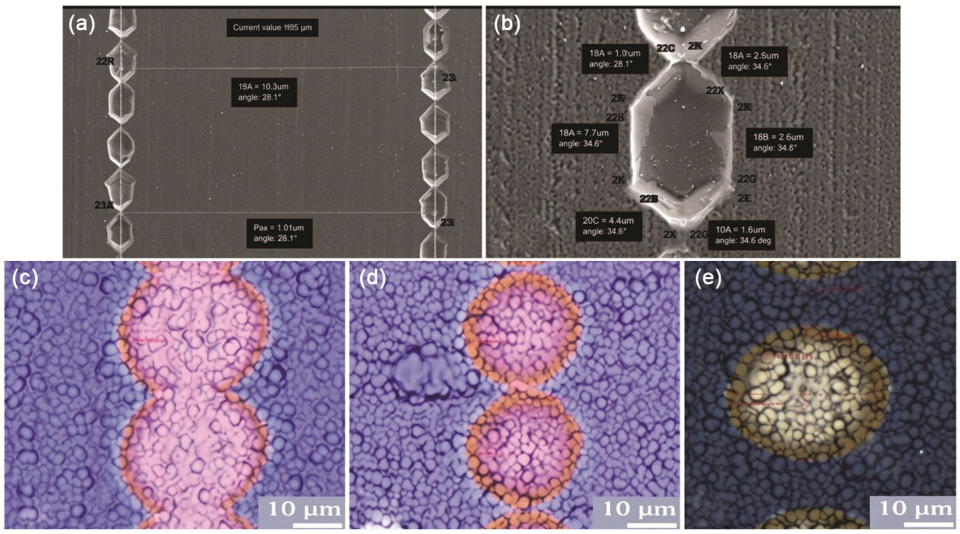


Fig. 6 — (a, b) Morphology of laser contact opening (LCO)− micrograph taken after removal of rear paste using HF, Variation of spot diameter with Laser speed; (c) Scan speed – 4 m/s, (d) Scan speed – 5 m/s, (e) Scan speed – 6 m/s

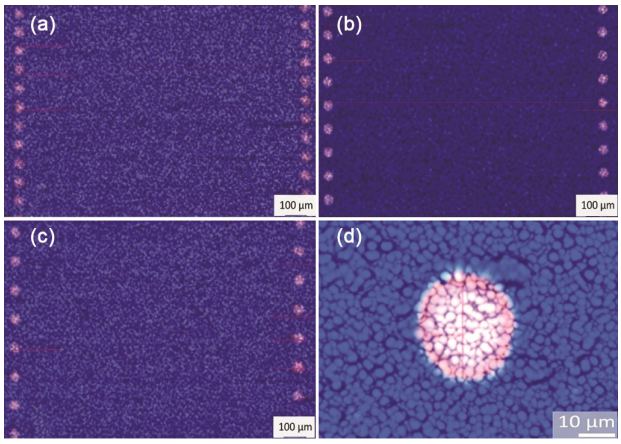


Fig. 7 — Laser Contact Opening (LCO) withdot pattern having dot size of 43 µm and varying distance between dots: (a) dot−dot distance 36 µm, Ablated area 1.5 % & MCLT 18.23µs; (b) dot−dot distance 54 µm, Ablated area 1.24 % & MCLT 27.87µs; (c) dot−dot distance 76 µm, Ablated area 0.98 % & MCLT 40.75µs

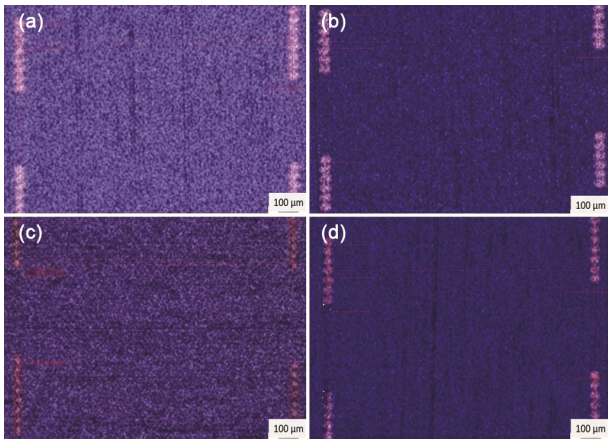


Fig. 8 — Laser Contact Opening (LCO) employed dash pattern having varying dash size of: (a) 328 µm, (b) 243 µm, (c) 322 µm, (d) 277 µm; dash gap: (a) 352 µm, (b) 355 µm, (c) 322 (µm d) 357 µm with a pitch of 1.1 mm; Result: (a) Ablated area – 1.96 % & MCLT – 39.86µs, (b) Ablated area – 1.62 % & MCLT – 57.66µs, (c) Ablated area – 1.42 % & MCLT – 62.01µs, (d) Ablated area – 1.26 % & MCLT – 62.15µs

resulted in variation of total ablated area from 1.5% to 0.98%. After screen printing and firing of these cells, they were studied for dependence of Minority Carrier Life Time (MCLT) on ablation area. The MCLT has been observed to be 18.23µs and 40.75µs for ablation area of 1.5% and 0.98%, respectively. This has been attributed to the decreasing ablation induced damage area with decreasing total ablation area. It can be simply concluded that minimum laser interaction with the substrate results in lesser metallurgical degradation in terms of heat affected zones, partial melting at the Local Contact Opening (LCO).

A continuous line or a dash pattern ablation was realized with scan speed of less than 4 m/s with a spot diameter of 43µm with 30% laser power. Morphology of dash pattern were studied under SEM (Fig. 6c) which clearly shows the dot having diffused edge. However, with scan speed of 5 m/s (Fig. 6d), a stage between dash and dot can be seen.

The ablation can be carried in different patterns which can include dot, dash, line and combination of line and dash. A clear dot structure having spot diameter of 43 µm was realized using a scan speed of 6 m/s with lower scan speeds leading to converging or overlapping of dots to form a line structure or getting diffused to each other. Therefore, a scan speed of 6 m/s was chosen to form a dot pattern during ablation (Fig. 6e).

The effect of variations in dash patterns with varied dash size and gap between dashes is also studied. Dash length was varied from 328µm to 277µm along with a dash gap variation from 352µm to 322µm. These variations led to variation in the ablated area and thus affected the MCLT (Fig. 7). After screen printing and firing of these cells, they were studied for Minority carrier life time to assess the quality of ablation. A significant change in MCLT has been observed from 39.86µs to 64.76µs for ablation area of 1.96% to 0.96% respectively. Similar to that observed in dot pattern, dash pattern also showed that decreasing the ablation area leading to decreased damage area and thus enhanced MCLT.

It is observed that though dash pattern has a higher ablation area than a dot pattern still dash pattern showed higher Minority Carrier Life time (MCLT) (Figs. 7, 8 and Table 3). This effect can be understood by analyzing the heat affected zone area variation in dash and dot patterns. While forming a dot pattern, it is expected to generate a heat affected zone around every dot however in case of a dash pattern, this is minimized, i.e., the heat affected zone area per unit area of ablation will be smaller in case of dash pattern as compared to a dot pattern.

After dielectric ablation, wafers were taken for front and rear contact printing using Ag paste and Silicon doped Al paste, respectively followed by co−firing of contacts to achieve a typical solar cell. The contact firing treatment followed is presented in Fig. 9. The firing profile for local contact formation is subdivided into three main steps: ramp−up, peak firing temperature, and cool down.

During the ramp−up phase, the temperature is increased from ambient to approximately 600°C over a

Table 3 — Effect of various parameter on MCLT

No	Laser power	laser speed (m/s)	Set dash length (mm)	Set dash gap (mm)	Pitch (mm)	Ablated area (%)	MCLT (μ−sec)
				Dot pattern			
1	30	8	0.04	0.036	1.1	1.5	18.23
2	30	10	0.04	0.052	1.1	1.24	27.87
3	30	12	0.04	0.076	1.1	0.98	40.75
4	20	12	0.04	0.076	1.1	0.98	32.93
				Dash pattern			
5	45	4	0.05	0.3	1.1	1.96	39.86
6	45	4	0.02	0.3	1.1	1.62	57.66
7	30	4	0.05	0.3	1.1	1.42	62.1
8	30	4	0.02	0.3	1.1	1.26	60.97
9	30	5	0.9	0.9	1.1	1.61	47.05
10	30	5	0.45	0.9	1.1	1.34	31.37
11	30	5	0.3	0.6	1.1	1.52	41.43
12	30	5	0.3	0.3	1.1	2.07	32.66
13	30	5	0.3	0.9	1.1	1.23	24.38
14	30	5	0.05	0.9	1.1	0.96	64.76
15	45	4	0.3	0.6	0.7	3.72	29.3

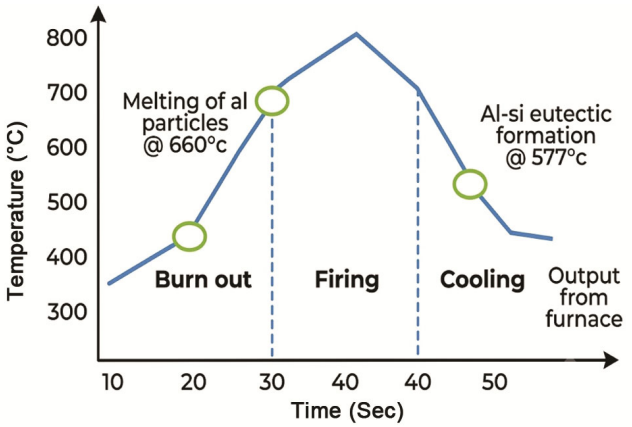


Fig. 9 — Typical firing profile for PERC solar cells

duration of about 30−40 seconds which can be changed by altering the belt speed. This step ensures the complete burnout of organic components in the paste, preparing the contact openings for subsequent reactions. At this stage, no significant interaction between aluminum (Al) and silicon (Si) occurs, as the temperature remains below the melting point of Al.

In the second phase, the peak firing temperature is reached, ranging from 660°C to approximately 800−900°C, lasting around 3 seconds. At 660°C, Al begins to melt, forming a liquid Al−Si alloy as Si starts dissolving into the molten Al. This dissolution process continues until the peak temperature is achieved, with higher temperatures promoting the uniform diffusion of Si into the molten Al matrix.

The final phase, cool down, involves reducing the temperature from the peak firing temperature back to ambient. During this phase, significant phase transformations occur as the system approaches the eutectic temperature while cooling down. As the temperature decreases, the solubility of Si in the liquid Al−Si alloy reduces, and Si begins to precipitate out of the Al−Si matrix. This phenomenon, known as solute rejection, is driven by the equilibrium constraints of the Al−Si binary phase diagram. After reaching the eutectic temperature of 577°C, the liquid Al−Si alloy solidifies into a two−phase microstructure consisting of Al and Si. During this transformation, Si segregates to the contact region, forming a continuous eutectic Al−Si layer. This layer provides the necessary electrical and mechanical connection for the contact formation. The cooling dynamics in the belt furnace play a critical role in determining the morphology and distribution of the Al and Si layers in the eutectic microstructure. If the cooling rate is rapid, the diffusion of Si back to the contact region may be incomplete, potentially resulting in non−uniform eutectic formation however, slower cooling allows sufficient time for Si atoms to diffuse and form a well−defined lamellar eutectic layer. However, the differences in diffusion rates of Si into Al and Al into Si, along with the rejection of excess Si during cooling, often lead to the formation of Kirkendall voids at the interface. As the Al−Si alloy cools and

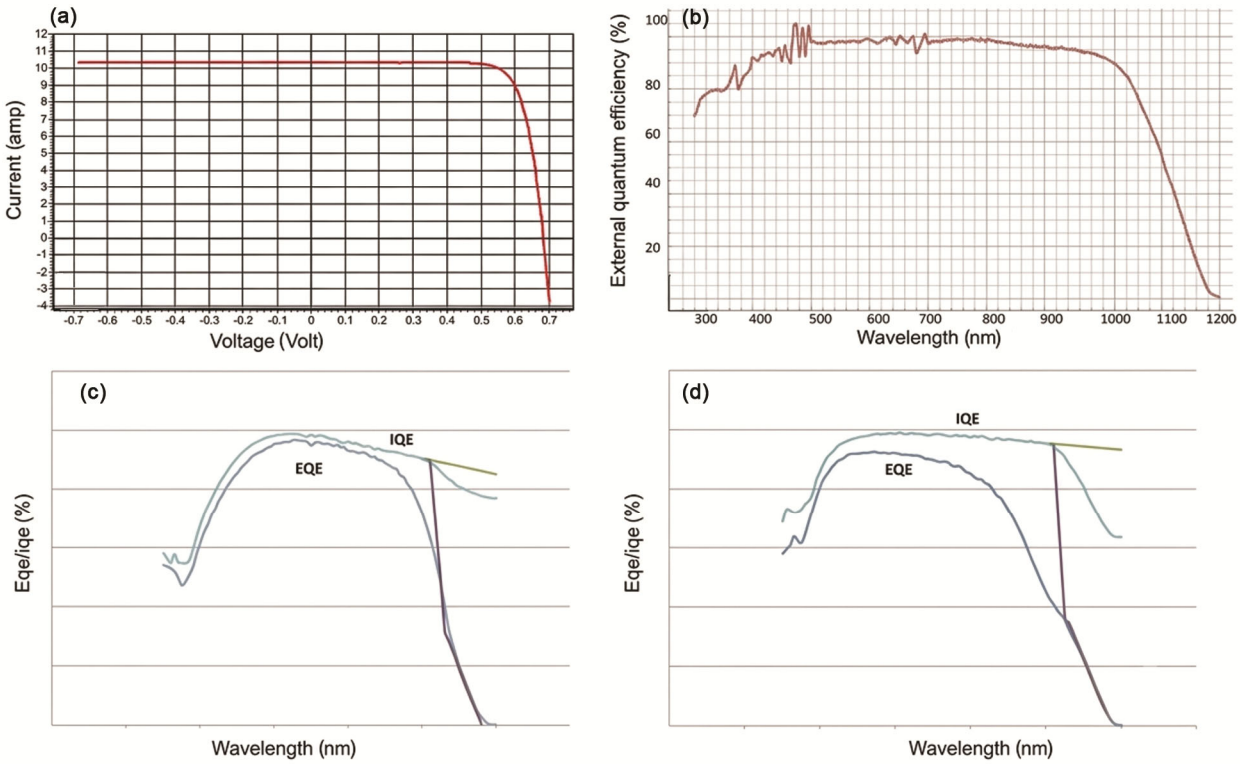


Fig. 10 — (a) IV Curve for PERC Cell having 22.07 % efficiency, fill factor 78.6%, (b) External quantum efficiency of the champion PERC cell, (c) Benchmark PERC cell, (d) Standard Al BSF cell

reaches its solid−state solubility limits, the excess Si migrates toward the contact region, leaving behind voids where Al cannot diffuse quickly enough to compensate for the material imbalance. To mitigate these issues, Si−doped Al paste is used in the present study, as alloyed Si in the paste reduces the diffusion gradients and prevents excessive Kirkendall void formation. This is in consistent with the studies of Singh.[13] This has helped in formation of a uniform eutectic layer formation across the LCO and resulted in higher open−circuit voltage (Voc), reduction in charge recombination and leading to better performance and reliability of the contact.

The firing profile was optimized independently following the optimized LCO parameters but in instances, feedback from metallization studies informed further refinement of the LCO process, as the characteristics of LBSF including Kirkindal void could be more accurately assessed post co−firing of contacts. Cross−sectional analysis using SEM provided clear insights into the LBSF formation enabling iterative optimization of the LCO parameters.

Quantum Efficiency (QE) measurements were performed to evaluate the spectral response and carrier collection characteristics of the fabricated cells in the 300–1200 nm range. The External Quantum Efficiency (EQE), representing the fraction of incident photons converted into electrical current, and the Internal Quantum Efficiency (IQE), which accounts only for absorbed photons, were analyzed to decouple optical and electrical losses. The PERC cell exhibited an efficiency of 22.07% with a fill factor of 78.6%, as confirmed by the IV characteristics in Fig. 10(a). A statistical analysis of 30 fabricated cells using UV picoseconds laser with a dot pattern, printed using knotless screen and using silicon doped paste on rear side indicate a mean efficiency of 21.14%, with a standard deviation of 0.46%, demonstrating a high degree of process uniformity. The efficiencies span a range from 20.03% to 22.07%, with the majority of devices clustered around ~21%, underscoring the reproducibility and stability of the fabrication process. The EQE spectrum revealed high responsivity (≥90%) (Fig. 10b) between 500–900 nm, while reduced EQE at short wavelengths (300–500 nm) indicated surface recombination at the emitter, and diminished response at longer wavelengths (900–1200 nm) suggested incomplete absorption and rear recombination. IQE analysis showed superior carrier collection in the PERC cell produced under the current study

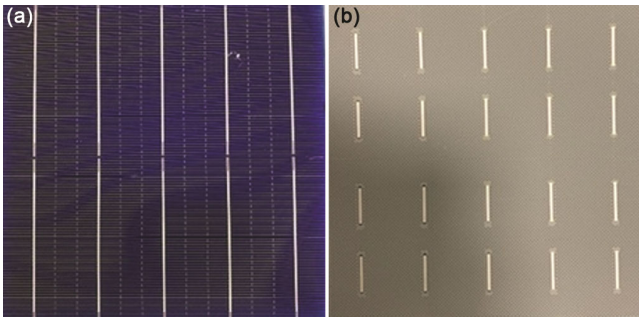


Fig. 11 — Screen printed wafer: (a) front surface (b) rear surface

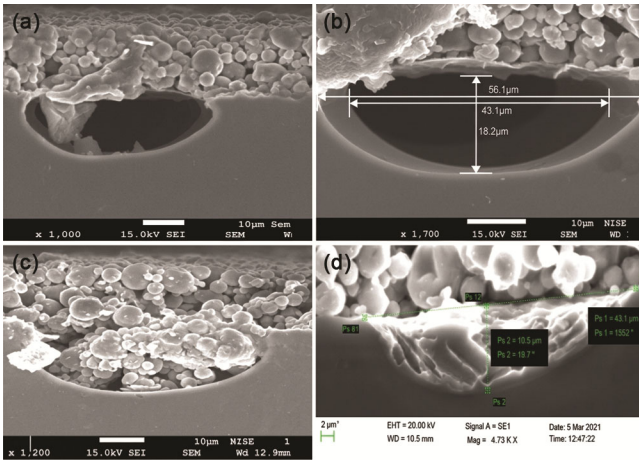


Fig. 12 — (a), (b) Cross−sectional SEM images of partial−filled local back surface field (LBSF) formed using silicon−free Al paste, showing the presence of a void (width: ~56 µm, depth: ~18 µm); (c) formation of a Kirkendall void and accumulation of paste residuals due to absence of eutectic formation with Si−free Al paste; (d) metallization using Si−doped Al paste resulting in a fully filled LBSF, free from voids, and exhibiting well−formed Al–Si alloy phases including eutectic, hypereutectic, and paste residuals.

(Fig. 10c**)** compared to a standard Al−BSF cell (Fig. 10d), particularly in the near−infrared region, attributable to improved rear surface passivation and enhanced optical confinement. The gap between EQE and IQE spectra was narrower in the PERC architecture, indicating reduced front−surface reflection and minimized recombination losses. These results collectively validate the efficacy of PERC design in enhancing photon absorption and carrier extraction, offering insights for further optimization of passivation schemes and light management strategies.

It has also been observed that when wafers are printed (Fig. 11) using a dash pattern along the screen printing direction have reported higher VoC and efficiency because of having lesser voids generation upon co−firing.

To suppress Kirkindal void formation, Si doped Al paste was used in this study which promoted the formation of Al−Si eutectic which upon cooling led to favorable lamellar microstructure at the LBSF. The effect of using Si doped Al paste on voids formation and contact establishment is evidenced in the cross−sectional fired contacts presented for Si doped and no Si doped Al paste (Fig. 12).

Conclusions

The findings of the laser ablation study demonstrate that employing a UV picosecond laser significantly reduces metallurgical damage while enhancing optical and electrical properties, as evidenced by improved MCLT. Further, the study underscores the importance of balancing key laser parameters such as power, speed, and ablation area to reduce substrate damage and maximize cell performance. A lower ablation area was strongly correlated with higher MCLT and improved overall efficiency. Combined with a precisely controlled firing profile, these optimizations culminated in a Mono PERC cell efficiency of 22.07%. The achieved fill factor (FF) is ~78.6% where the typical FF ranges from 76−80% corresponding to the process conditions and resistive losses. FF value obtained din this study suggesting effective optimization of contact formation, minimizing recombination, resistive losses thereby validating the efficacy of proposed LCO and firing strategies. The results in the present study also suggest potential ways for further enhancement efficiency through précised laser ablation geometries and PECVD deposition techniques. This study paves path for potential future work focusing on finite element−based thermal modelling, HAZ mapping for LCO geometries, advanced tool including µ−PCD, TEM to be employed to quantify microstructure features, defect dynamics, and carried recombination. In addition, co−optimization of laser parameters with emitter formation and metallization along with quantitative void analysis, reliability testing, shall become crucial for validation, scalability and industrial applicability of the approach as equipment(s) used in the present study are having industrial scale throughput.

Acknowledgment

We sincerely acknowledge the support provided by National Institute of solar Energy, Indian Institute of Technology Roorkee, Bharat Heavy Electricals Limited Hardwar for testing and characterization. We

express our sincere gratitude to Ministry of New and Renewable Energy (MNRE) India for funding the prestigious research for developing Passivated Emitter Rear Contact (PERC) technology indigenously.

Funding Information

This work was supported by [Ministry of New and Renewable Energy, Government of India] (Grant numbers [31/39/2015−16/PVSE−R&D]. Authors have received research support from Ministry of New and Renewable Energy, Government of India.

Conflict of Interest

The authors have no relevant financial or non−financial conflict of interests to disclose. All authors contributed to the study conception and design. Material preparation, data collection and analysis were performed by Devdutt Singh, Dr. Sai Ram Meka, Himadri Agarwal and Dr. Bharat K Pant. The first draft of the manuscript was written by Devdutt Singh and all authors commented on previous versions of the manuscript. All authors read and approved the final manuscript.

References

1 F Qian, H Shen, G Huang, B Liu & J Hong, Improvement of laser−induced damage on high−efficiency solar cells via top−hat beam ablation, *Energies*, **17** (2024) 858.

2 Kim M S, Lee J H & Kwak M K, Review: Surface texturing methods for solar cell efficiency enhancement, *Int J Precis Eng Manuf*, **21** (2020) 1389–1398.

3 Salman K A, Effect of surface texturing processes on the performance of crystalline silicon solar cell, *Sol Energy*, **147** (2017) 228–231.

4 Hwang Y, Park C, Kim J, Kim J, Lim J Y, Choi H, Jo J & Lee E, Effect of laser damage etching on i−PERC solar cells, *Renew Energy*, **79** (2015) 131–134.

5 Balaji N, Lai D, Shanmugam V, Basu P K, Khanna A, Duttagupta S & Aberle A G, Pathways for efficiency improvements of industrial PERC silicon solar cells, *Sol Energy*, **214** (2021) 101–109.

6 Hallam B, Urueña A, Russell R, Aleman M, Abbott M, Dang C, Wenham S, Tous L & Poortmans J, Efficiency enhancement of i−PERC solar cells by implementation of a laser doped selective emitter, *Sol Energy Mater Sol Cells*, **134** (2015) 89–98.

7 Carlson D E, Laser processing of solar cells, *Proc SPIE*, **8473** (2012) 847302.

8 Sato Y, Ishikawa Y & Nakamura M, Efficiency improvement in p−type PERC solar cells by laser ablation process, *Sol Energy Mater Sol Cells*, **136** (2015) 46–51.

9 Wu H, Zhao S, Hong J, Zou D, Hu K, Zhu P & Chen Y, Performance optimization of PERC solar cells based on laser ablation forming local contact on the rear, *High Temp Mater Process*, **43(1)** (2024) 20220326.

10 Jaeger K & Hezel R, A novel thin silicon solar cell with Al_2O_3 as surface passivation, *Proc 8th IEEE Photovolt Specialist Conf* (1985) 1752–1753.

11 Suh D, Influence of laser damage and contact geometry on the performance of passivated emitter and rear cell solar cells, *Thin Solid Films*, **668** (2018) 45–49.

12 Kim J, Kim J, Lim J Y, Hwang Y, Cho J, Choi H & Lee E, Laser ablation of aluminum oxide and silicon nitride rear−side passivation for i−PERC cell, *Renew Energy*, **79** (2015) 135–139.

13 Singh D, Agrawal H, Pant B K, Singh V K, Shrivastava P & Kumar R, Qualitative damage assessment of laser contact opening and microstructural evolution at the rear contact of a PERC mono crystalline Si solar cell upon co−firing with Si doped Al paste, *J Inst Eng India Ser D*, **104** (2023) 767–776.

14 Kuo C W & Kuan T M, Impact of laser opening ratio for mass production high efficiency mono−crystalline silicon solar cells, *Proc 29th European Photovolt Sol Energy Conf Exhibit (2014*).

15 Chiu J S, Zhao Y M, Zhang S & Wuu D S, The role of laser ablated backside contact pattern in efficiency improvement of mono crystalline silicon PERC solar cells, *Sol Energy*, **196** (2020) 462–467.

16 Urrejola E, Understanding and avoiding the formation of voids for rear passivated silicon solar cells, *Proc 3rd Workshop Metallization Crystalline Silicon Solar Cells (2011).*

17 Singh D, Pant B K, Bhardwaj V & Pillai P S, Optimization of texturisation parameters for enhanced efficiency of PERC type solar cell produced using diamond wire saw wafers, *J Inst Eng India Ser D* (2025).

18 Singh A, Umakanth V, Tyagi N, Baghel A K & Kumar S, Comparative study of commercial crystalline solar cells, *Results Opt*, **11** (2023) 100379.